Magnetic properties of $PrMn_{2-x}Fe_xGe_2$—^{57}Fe Mössbauer spectroscopy

2006 J. Phys.: Condens. Matter 18 189

(http://iopscience.iop.org/0953-8984/18/1/014)

INSTITUTE OF PHYSICS PUBLISHING JOURNAL OF PHYSICS: CONDENSED MATTER

J. Phys.: Condens. Matter **18** (2006) 189–204 doi:10.1088/0953-8984/18/1/014

Magnetic properties of $PrMn_{2-x}Fe_xGe_2$—^{57}Fe Mössbauer spectroscopy

J L Wang[1], S J Campbell[1], J M Cadogan[2], O Tegus[3], A J Studer[4] and M Hofmann[5]

[1] School of Physical, Environmental and Mathematical Sciences, The University of New South Wales, The Australian Defence Force Academy, Canberra ACT 2600, Australia
[2] School of Physics, The University of New South Wales, Sydney, NSW 2052, Australia
[3] Van der Waals-Zeeman Institute, University of Amsterdam, 1018 XE Amsterdam, The Netherlands
[4] Bragg Institute, ANSTO, Lucas Heights, NSW, Australia
[5] Technische Universität München, FRM-II, 85747 Garching, Germany

Received 2 August 2005, in final form 9 November 2005
Published 9 December 2005
Online at stacks.iop.org/JPhysCM/18/189

Abstract

We have investigated the magnetic behaviour of $PrMn_{2-x}Fe_xGe_2$ compounds with $x = 0.4$, 0.6 and 0.8 over the temperature range 4.2–350 K using ac magnetic susceptibility, dc magnetization and ^{57}Fe Mössbauer effect spectroscopy, as well as neutron diffraction for the $PrMn_{1.2}Fe_{0.8}Ge_2$ compound. Replacement of Mn with Fe leads to contraction of the unit cell and a shortening of the Mn–Mn spacing, resulting in modification of the magnetic structure. $PrMn_{1.6}Fe_{0.4}Ge_2$ is an intralayer antiferromagnet at room temperature and ferromagnetic below $T_C^{inter} \sim 230$ K with additional ferromagnetic ordering of the Pr sublattice detected below $T_C^{Pr} \sim 30$ K. Re-entrant ferromagnetism has been observed in $PrMn_{1.4}Fe_{0.6}Ge_2$ with four magnetic transitions ($T_N^{intra} \sim 333$ K, $T_C^{inter} \sim 168$ K, $T_N^{inter} \sim 152$ K and $T_C^{Pr} \sim 40$ K). Moreover, it was found that T_C^{inter} and T_C^{Pr} increase with applied field while T_N^{inter} decreases. $PrMn_{1.2}Fe_{0.8}Ge_2$ is antiferromagnetic with $T_N^{intra} \sim 242$ K and $T_N^{inter} \sim 154$ K. The magnetic transition temperatures for all compounds are also marked by changes in the ^{57}Fe magnetic hyperfine field and the electric quadrupole interaction parameters. The ^{57}Fe transferred hyperfine field at 4.5 K in $PrMn_{1.6}Fe_{0.4}Ge_2$ and $PrMn_{1.4}Fe_{0.6}Ge_2$ is reduced (below the ordering temperature of the Pr sublattice) compared with that at 80 K (above T_C^{Pr}), indicating that the transferred hyperfine field from Pr acts in the opposite direction to that from the Mn atoms. The neutron data for $PrMn_{1.2}Fe_{0.8}Ge_2$ demonstrate that an anisotropic thermal expansion occurs within the interplanar antiferromagnetic range.

(Some figures in this article are in colour only in the electronic version)

1. Introduction

RMn_2X_2 (R = rare earths, X = Ge, Si) compounds with the tetragonal $ThCr_2Si_2$-type structure (space group $I4/mmm$) exhibit a range of interesting phenomena including mixed valence and heavy fermion behaviour as well as various types of magnetic phase transitions: paramagnetic (P) to ferromagnetic (F), P to antiferromagnetic (AF), F to AF, AF to F [1]. In this structure, the R, Mn and Ge atoms lie in alternate layers stacked along the c-axis according to the sequence . . .R–Ge–Mn2–Ge–R. . .. The R and Mn layers are square planes with Mn–Mn and R–R separations of ∼0.28 and ∼0.4 nm, respectively and with an interplanar spacing around ∼0.52 nm. All of the atoms are located at special positions: R at 2a $(0, 0, 0)$, Mn at 4d $(1/2, 0, 1/4)$ and Ge at 4e $(0, 0, z)$. The value of z is close to 0.37, with interlayer and intralayer distances depending mainly on the a and c parameters [1]. The Mn-based compounds have attracted particular interest because the Mn atoms carry a magnetic moment. Magnetic ordering of the Mn sublattice generally persists to temperatures above 300 K while the rare earth sublattice orders magnetically at low temperatures (e.g. [2, 3]).

It is well known that the magnetic properties of $RMn_2(Ge, Si)_2$ compounds are sensitive to the interatomic distances and that the resulting magnetic structures arise from the interplay between the R–Mn and Mn–Mn exchange interactions [2]. The magnetic properties of these compounds are very sensitive to the intralayer Mn–Mn spacing d^a_{Mn-Mn} and three general categories can be delineated:

(i) $d^a_{Mn-Mn} > 0.287$ nm ($a > 0.406$ nm)—the intralayer in-plane coupling is AF and the interlayer coupling is F;
(ii) 0.284 nm $< d^a_{Mn-Mn} < 0.287$ nm (0.402 nm $< a < 0.406$ nm)—the intralayer in-plane coupling is AF and the interlayer coupling is also AF—and
(iii) $d^a_{Mn-Mn} < 0.284$ nm ($a < 0.402$ nm)—there is effectively no intralayer in-plane spin component and the interlayer coupling remains AF [4].

Due to the strong dependence of the interlayer Mn–Mn exchange interaction on the lattice constant a, the value of d^a_{Mn-Mn} can be varied around the critical value by mixing either the rare-earth or the transition metal (T) atoms. This leads to a variety of magnetic properties in these systems with a range of different types of F and AF phases observed [1–6]. In order to have a deeper understanding of the volume dependence of the magnetic phase transitions in the RMn_2X_2 series, it is important to investigate a solid solution for which the thermal evolution of the a parameter goes through the critical value of 0.402 or 0.406 nm, namely $d_{Mn-Mn} = 0.284$ or 0.287 nm. Recently, Kervan *et al* [7] reported that substitution of Mn by Fe in $PrMn_{2-x}Fe_xGe_2$ leads to re-entrant F order at $x \sim 0.6$; Kervan *et al* also constructed a partial magnetic phase diagram for $PrMn_{2-x}Fe_xGe_2$. Moreover, similar re-entrant $SmMn_2Ge_2$-like magnetic behaviour was also observed in $NdMn_{2-x}Fe_xGe_2$ [6]. By comparison, this type of magnetic behaviour is not observed in $PrMn_{2-x}Co_xGe_2$ [8] and $NdMn_{2-x}Co_xGe_2$ [9] even though the lattice constant a is almost the same in $PrMn_{2-x}Co_xGe_2$, $NdMn_{2-x}Co_xGe_2$, $PrMn_{2-x}Fe_xGe_2$ and $NdMn_{2-x}Fe_xGe_2$. This difference in behaviour indicates that the interplanar coupling is not determined solely by geometric criteria. Electronic effects also play a role in determining the magnetic behaviour of the RMn_2X_2 system, as suggested by the ferromagnetic interlayer exchange observed in UMn_2Ge_2 (despite the short Mn–Mn separation distance ($d = 0.2837$ nm) [10]), and by the observation that only the AFl magnetic structure is detected over the entire range of order in $CaMn_2Ge_2$ and $BaMn_2Ge_2$ with $d > 0.294$ nm [11].

As demonstrated in earlier studies of RMn_2X_2 systems, Mössbauer spectroscopy measurements on ^{57}Fe doped samples [12, 13] and/or neutron diffraction measurements [13–15] enable magnetic phase transitions to be determined which might otherwise be overlooked if only bulk

Table 1. Lattice parameters and structural information for the $PrMn_{2-x}Fe_xGe_2$ compounds ($x = 0.4$–0.8) at room temperature (the errors for the lattice parameters a and c, and the interatomic spacing distances, were derived to be ± 0.0001 nm from the data fits; z_{Ge}, ± 0.001).

x	d_{Mn-Mn} (nm)	d_{Mn-Ge} (nm)	d_{Mn-Pr} (nm)	d_{Pr-Ge} (nm)	d_{Pr-Pr} (nm)	d_{Ge-Ge} (nm)	a (nm)	c (nm)	V (nm^3)	z_{Ge}	Reference
0	0.2915	0.2510	0.3422	0.3192	0.4123	0.2600	0.4123	1.0925	0.1857	0.381	[14]
0.4	0.2899	0.2486	0.3404	0.3182	0.4100	0.2622	0.4100	1.0869	0.1827	0.379	
0.6	0.2891	0.2531	0.3393	0.3136	0.4088	0.2433	0.4088	1.0834	0.1811	0.388	
0.8	0.2886	0.2486	0.3387	0.3159	0.4082	0.2568	0.4082	1.0813	0.1801	0.381	
2	0.2834						0.4057	1.0517	0.1732		[13]

magnetic measurements are carried out. Moreover, given that several aspects of the magnetic behaviour of the $PrMn_{2-x}Fe_xGe_2$ system remain unknown, particularly the existence of three regions of qualitatively different magnetic behaviour [7], here we investigate the effect of replacing Mn atoms by Fe atoms on the magnetic properties and structure of $PrMn_{2-x}Fe_xGe_2$ using magnetization and ^{57}Fe Mössbauer spectroscopy measurements, augmented by initial neutron diffraction analysis.

2. Experimental details

Polycrystalline samples of $PrMn_{2-x}Fe_xGe_2$ with $x = 0.4$, 0.6 and 0.8 were synthesized by arc melting the high purity elements on a water-cooled Cu hearth under purified argon gas. The mass loss of Mn during melting was compensated for by adding 2% excess Mn. The samples were doped with ~3.5 at.% enriched ^{57}Fe to enhance the sensitivity of the ^{57}Fe Mössbauer experiments. The ingots were melted five times to attain homogeneity and then annealed at 900 °C for one week in an evacuated quartz tube. The samples were characterized by x-ray diffraction (Cu Kα radiation, $\lambda = 0.154\,18$ nm). The temperature dependence of the ac magnetic susceptibility (frequency range $f = 33$–333 Hz and $H_{ac} = 78$ A m^{-1}) was measured using a standard, variable temperature helium cryostat and a computer controlled Lakeshore Cryogenics temperature controller (4.2–300 K). The temperature dependence of the magnetization was measured in a magnetic field of 0.05 T in a superconducting quantum interference device (SQUID) from 5 to 350 K after first cooling in zero field. The magnetic transition temperatures have been determined with an accuracy of ± 5 K. ^{57}Fe Mössbauer spectra were obtained between 4.2 and 298 K using a standard constant-acceleration spectrometer and a ^{57}CoRh source. The spectra were calibrated at room temperature with an α-Fe foil. Neutron diffraction experiments were carried out on the $PrMn_{1.2}Fe_{0.8}Ge_2$ sample using the HRPD and MRPD diffractometers at Reactor HIFAR, Lucas Heights, over the temperature range ~20–300 K.

3. Results and discussion

The room temperature x-ray diffraction patterns show that all of the compounds investigated here are single phase and crystallize in the $ThCr_2Si_2$-type structure with no evidence of any impurity phases. The x-ray data were refined using the FULLPROF program [16] and the results of the refinements for all compounds are listed in table 1. The lattice constants and the unit cell volume decrease monotonically with increasing Fe composition, reflecting the smaller atomic size of Fe compared to Mn. The lattice constants of $PrMn_{2-x}Fe_xGe_2$ are in good agreement with previously reported values [7]. The bond lengths between different sites have also been calculated with the BLOKJE program [17] using the structural and positional

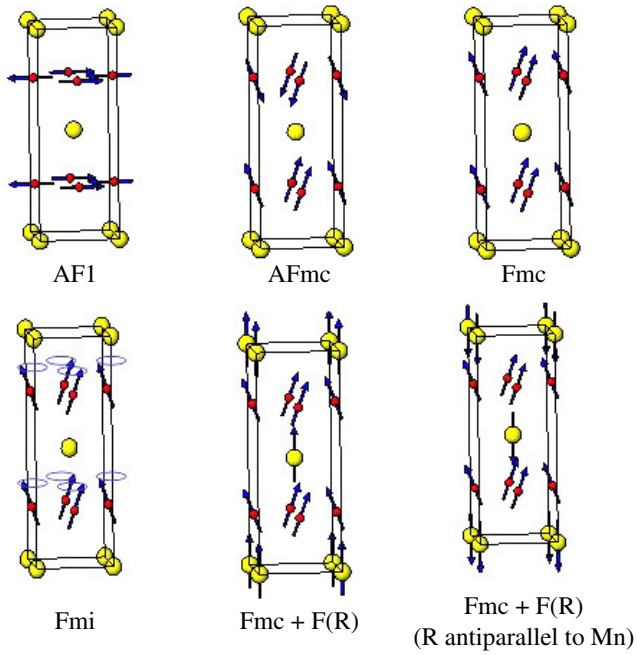

Figure 1. The magnetic structures relevant to discussion of the $PrMn_{2-x}Fe_2Ge_2$ compounds (the R and Mn atoms are shown as large and small circles respectively; for clarity the Ge atoms are not shown). The different structure types are defined in [3] and [5].

parameters and the 12-coordinate metallic radii of 0.182, 0.126, 0.135 and 0.137 nm for Pr, Fe, Mn and Ge, respectively. As is clear from the data in table 1, the decrease in the lattice parameters with increasing Fe content, x, results in a decrease of the intralayer nearest Mn–Mn distance $d^a_{\mathrm{Mn-Mn}}$ and the interlayer nearest Mn–Mn distance $d^c_{\mathrm{Mn-Mn}}$.

3.1. Magnetic studies

In order to discuss more readily the magnetic behaviour observed in this study, several of the Mn sublattice magnetic structures related to the $PrMn_{2-x}Fe_xGe_2$ system are depicted in figure 1. The notation used to describe the different structure types is defined in [3, 5].

The temperature dependences of the magnetization of the $PrMn_{2-x}Fe_xGe_2$ compounds ($x = 0.4$, 0.6 and 0.8) over the temperature range 5–350 K in an applied field of $B_{\mathrm{appl}} = 0.05$ T are shown in figures 2(a), 3(a) and 4(a), respectively. The magnetization curves for applied fields up to $B_{\mathrm{appl}} = 5$ T at selected temperatures are shown in figures 2(b), 3(c) and 4(c).

3.1.1. $PrMn_{1.6}Fe_{0.4}Ge_2$. As is evident from figure 2(a) and in good agreement with earlier results [7], there are two magnetic phase transitions in $PrMn_{1.6}Fe_{0.4}Ge_2$, at ∼230 and ∼30 K. It has been reported [12, 14] that $PrMn_2Ge_2$ first exhibits a transition from paramagnetism to an intralayer in-plane antiferromagnetic state (AFl) at $T_{\mathrm{N}}^{\mathrm{intra}} = 415$ K with decreasing temperature, then a canted spin structure appears with the c-axis interlayer spin components aligning parallel (Fmc) when the temperature is cooled below $T_{\mathrm{C}}^{\mathrm{inter}} = 334$ K. The magnetic structure transforms from a canted to a conical configuration (Fmi) below $T_{c/c} = 280$ K and the c-axis interlayer alignment remains parallel. Finally, below about 100 K the Pr sublattice

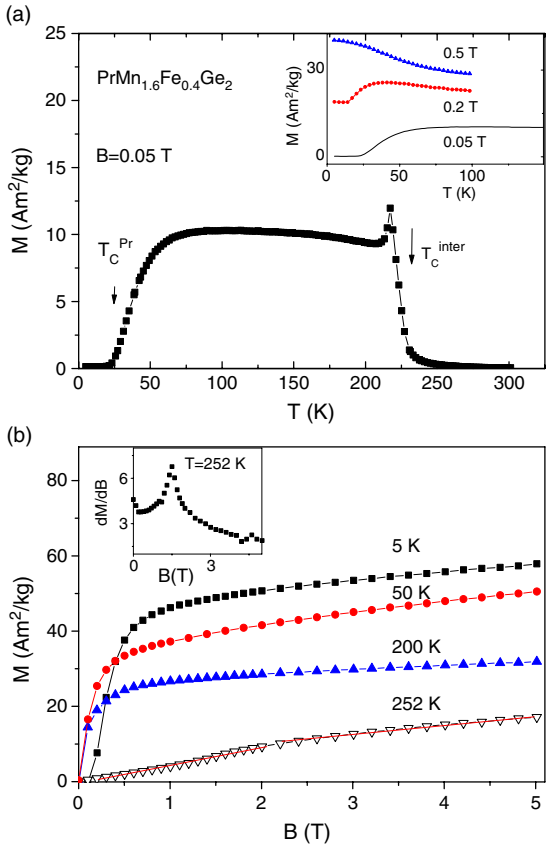

Figure 2. (a) The temperature dependence of magnetization ($B_{\rm appl}$ = 0.05 T) for $PrMn_{1.6}Fe_{0.4}Ge_{2.0}$. The inset shows M–T curves at various magnetic fields as discussed in the text. (b) The variation of magnetization with applied magnetic field ($B_{\rm appl}$ = 0–5 T) for $PrMn_{1.6}Fe_{0.4}Ge_{2.0}$ at the temperatures indicated. The inset shows the dM/dB versus B curve at 252 K.

in $PrMn_2Ge_2$ orders magnetically along the c-axis with the Pr moments coupled parallel to the Mn moments [12, 14]. By comparison, $PrFe_2Ge_2$ exhibits AF ordering of the Pr sublattice below T_N^{Pr} = 14 K [13] with the easy axis of magnetization along the c-axis. Moreover, it is well known that when Mn is replaced by another 3d element in RMn_2Ge_2, the magnetic ordering temperatures associated with the Mn sublattice decrease with increasing amounts of the substituting transition metal [6–9].

Following on from the behaviour of the limiting $PrMn_2Ge_2$ compound, we ascribe the transition at ∼30 K in $PrMn_{1.6}Fe_{0.4}Ge_2$ to the magnetic contribution (T_C^{Pr}) of the Pr sublattice [14]. Also, as discussed more fully below, in light of the analysis of our Mössbauer spectra for $PrMn_{1.6}Fe_{0.4}Ge_2$ (figure 5), the transition at ∼230 K is considered to correspond to an F to AF transition rather than an F to P transition. On this basis we therefore conclude that the transition in $PrMn_{1.6}Fe_{0.4}Ge_2$ at ∼230 K corresponds to the equivalent T_C^{inter} magnetic phase transition in $PrMn_2Ge_2$ from the higher temperature intralayer in-plane antiferromagnetic state to the lower temperature mixed ferromagnetic (Fmc) state for which, as is evident in figure 1, the intralayer in-plane coupling is AF and the interlayer coupling is F. In developing this

analogy, a further transition is therefore expected to occur in $PrMn_{1.6}Fe_{0.4}Ge_2$ from *a*–*b* plane AF to P somewhere in the region ∼350–∼415 K (this latter temperature corresponds to the T_N^{intra} transition in $PrMn_2Ge_2$). Unfortunately, temperatures above 300 K were not available during our experiment on $PrMn_{1.6}Fe_{0.4}Ge_2$ and we could not confirm this expectation directly.

On the basis of the overall magnetization curve and transition temperatures revealed in figure 2(a), the magnetic behaviour of $PrMn_{1.6}Fe_{0.4}Ge_2$ has been investigated further by measuring the magnetization curves at various temperatures as shown in figure 2(b). It is clear that below the transition at $T_C^{Pr} \sim 30$ K, the Pr sublattice gives a positive magnetic contribution to the Mn sublattice, reinforcing the ferromagnetic alignment of the Pr and Mn sublattices. This ferromagnetic character is also evident from the magnetization versus magnetic field (M–B) curve at 5 K (figure 2(b)). By comparison, the M–B curve of $PrMn_{1.6}Fe_{0.4}Ge_2$ at 252 K reflects the AF character of this compound above the transition at $T_C \sim 230$ K. A field-induced metamagnetic phase transition from AF to F has been detected at around 1.5 T at 252 K; this transition is evident from the dM/dB versus B curve shown in the inset to figure 2(b). This suggests that the ferromagnetic ordering of $PrMn_{1.6}Fe_{0.4}Ge_2$ can be shifted to higher temperatures by an applied magnetic field as we have observed for $PrMn_{1.4}Fe_{0.6}Ge_2$ (see below). The relatively low magnetization obtained for $PrMn_{1.6}Fe_{0.4}Ge_2$ below ∼25 K (figure 2(a); warming curve following initial cooling in zero field) in a field of 0.05 T can be understood in terms of the magneto-history effect resulting from narrow-domain-wall pinning [18]; this effect occurs when a large ratio of the anisotropy energy to the exchange energy is satisfied. In order to confirm this behaviour we also measured the M–T curves under various fields. As shown in the inset to figure 2(a), this anomaly, i.e. the rapid decrease of magnetization at low temperatures, disappears in high applied fields ($B = 0.5$ T) as expected.

The lattice parameter *a* for $PrMn_{1.6}Fe_{0.4}Ge_2$ at room temperature is 0.4100 nm and, as mentioned, the compound is AF at this temperature. However, with decreasing temperature the unit cell contracts and condition (i) (as discussed in the introduction) can be satisfied, resulting in the occurrence of interlayer Mn–Mn F ordering at $T_C \sim 230$ K. Even though the unit cell may continue to contract with decreasing the temperature to 5 K, the interlayer Mn–Mn F ordering is maintained, indicating that condition (i) remains satisfied. On the basis of condition (i), at some temperature $PrMn_{1.6}Fe_{0.4}Ge_2$ would be expected to exhibit the F mixed commensurate magnetic structure, F*mc*, which, as noted above, is characterized by the F interplanar coupling of the in-plane F components and the commensurate arrangement of the AF in-plane components. On increasing the temperature from the F*mc* magnetic range, the ferromagnetic interlayer coupling would disappear at temperature T_C^{inter}; only the antiferromagnetic interlayer Mn–Mn exchange interaction would exist above T_C^{inter} and therefore the compound should exhibit the AF*l* magnetic structure. On increasing the temperature above T_C^{inter}, a further magnetic phase transition from AF to P is expected at T_N^{intra}. $PrMn_{1.6}Fe_{0.4}Ge_2$ at room temperature just satisfies the AF*l* condition mentioned above. With decreasing temperature the unit cell contracts (but the *a* lattice parameter remains above 0.406 nm) and, as expected, interlayer Mn–Mn ferromagnetic ordering is observed at $T_C^{inter} \sim 230$ K.

3.1.2. $PrMn_{1.4}Fe_{0.6}Ge_2$. As shown in figure 3(a), the temperature dependence of the magnetization for $PrMn_{1.4}Fe_{0.6}Ge_2$ reveals the presence of four magnetic transitions, similar to the case of $SmMn_2Ge_2$ [19–22]. Likewise, the low field ac magnetic susceptibility measurements (figure 3(b)) exhibit the same overall temperature dependence as the magnetization data. The existence of a magnetic phase transition above room temperature is evident from the temperature dependence of the inverse of the magnetization over the temperature range ∼250–350 K (inset to figure 3(a)). Based on the magnetic structures of $PrMn_2Ge_2$ [12, 14] and the similarity in magnetic behaviour of $PrMn_{1.4}Fe_{0.6}Ge_2$ to that

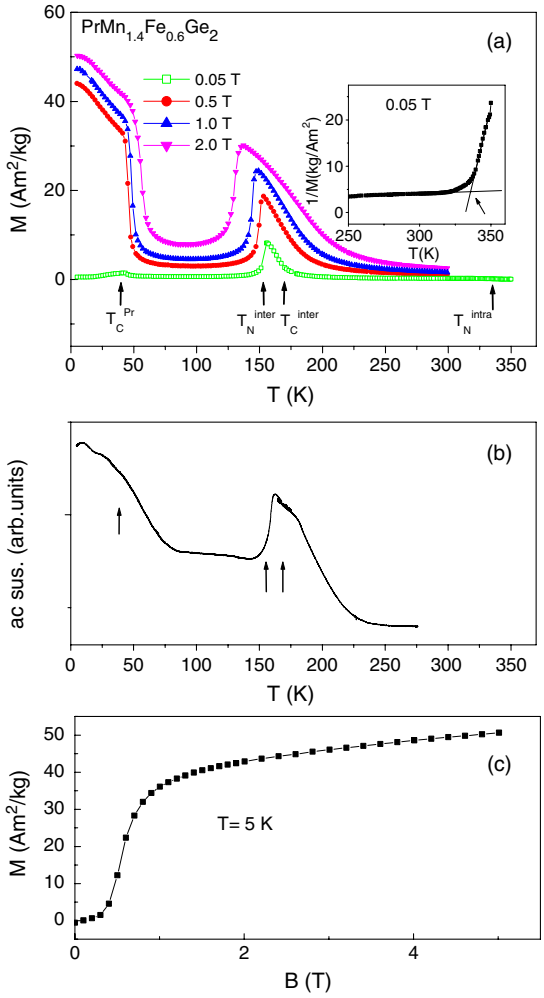

Figure 3. (a) The temperature dependence of magnetization for $PrMn_{1.4}Fe_{0.6}Ge_{2.0}$ at the magnetic fields indicated. The inset shows the inverse magnetization (B_{appl} = 0–5 T) of $PrMn_{1.4}Fe_{0.6}Ge_{2.0}$ over the temperature range 250–350 K. (b) The temperature dependence of the ac magnetic susceptibility (H_{rms} = 78 A m^{-1}; f = 133 Hz). (c) The variation of magnetization with applied magnetic field (B_{appl} = 0–5 T) for $PrMn_{1.4}Fe_{0.6}Ge_{2.0}$ at 5 K.

of $SmMn_2Ge_2$ [19–22], it can be concluded that with decreasing temperature from 350 K, $PrMn_{1.4}Fe_{0.6}Ge_2$ exhibits a transition from paramagnetism to an a–b plane antiferromagnetic state at around $T_N^{intra} \sim 333$ K (this transition is clearly higher than that derived from the partial magnetic phase diagram [7] but agrees with the extended results in [23]). This planar antiferromagnetism gives way to a c-axis ferromagnetic state at around $T_C^{inter} \sim 168$ K. With further decrease in temperature, a c-axis AF state occurs at around $T_N^{inter} \sim 152$ K and, finally, there is a transition to a c-axis F state with an additional Pr magnetic contribution at $T_C^{Pr} \sim 40$ K. The lattice parameter a in $PrMn_{1.4}Fe_{0.6}Ge_2$ at room temperature is 0.4088 nm which is slightly larger than that in $Nd_{0.35}La_{0.65}Mn_2Si_2$ [∼0.4070 nm, 5] and $SmMn_2Ge_2$ [∼0.4045 nm, 22], both of which exhibit similar magnetic behaviour. This common magnetic behaviour for disparate values of the lattice parameter a may be related to electronic effects as suggested in

the case of $NdMn_{1.6}Fe_{0.4}Ge_2$ for which the ferromagnetic to antiferromagnetic transition takes place at a larger d_{Mn-Mn} distance than in the pure $NdMn_2Ge_2$ compound [6].

For $GdMn_2Ge_2$ the lower temperature F state is driven by magnetic ordering of the Gd sublattice [12]; this behaviour also occurs in the present case of $PrMn_{1.4}Fe_{0.6}Ge_2$ where the Pr sublattice is considered to drive the low temperature F order. As evident from the thermomagnetic curves at different applied fields (figure 3(a)) the width of the lower temperature AF phase region decreases with applied magnetic field. This behaviour demonstrates that the applied magnetic field destroys the AF state in $PrMn_{1.4}Fe_{0.6}Ge_2$ (this has also been confirmed by the appearance of field-induced metamagnetic phase transitions in magnetization curves at 40 and 150 K [7]). It is well known that in RMn_2Ge_2 compounds even slight variations in the unit-cell parameters due to external factors such as pressure, field, temperature or chemical substitution are sufficient to modify the interlayer Mn–Mn spacing, leading to magnetic phase transitions (e.g. [22]). Such transitions are likely to be accompanied by an anomaly in the thermal expansion (magneto-volume effect) and can therefore be controlled by application of pressure or field. It has been reported that the width of the lower temperature AF phase region in $SmMn_2Ge_2$ can be extended by applied hydrostatic pressure [22]. The present results demonstrate that an applied magnetic field has the opposite effect to that of applied pressure; this behaviour can be understood in terms of magnetostriction. Figure 3(c) shows that $PrMn_{1.4}Fe_{0.6}Ge_2$ at 5 K becomes a standard ferromagnet similar to $PrMn_{1.6}Fe_{0.4}Ge_2$ and that the spontaneous magnetization of $PrMn_{1.4}Fe_{0.6}Ge_2$ at 5 K is lower than that for $PrMn_{1.6}Fe_{0.4}Ge_2$.

As in the case of $PrMn_{1.6}Fe_{0.4}Ge_2$, the lattice parameter a (0.4088 nm) of $PrMn_{1.4}Fe_{0.6}Ge_2$ at room temperature is larger than the critical value appropriate to condition (i) and the compound is antiferromagnetic. With decreasing temperature the unit cell contracts leading to the formation of the Fmc magnetic structure at $T_C^{inter} \sim 168$ K. The unit cell contracts with further decreases in temperature until at $T_N^{inter} \sim 152$ K condition (i) is no longer satisfied. $PrMn_{1.4}Fe_{0.6}Ge_2$ is now governed by condition (ii) and a magnetic transition from Fmc to AFmc is expected, consistent with the present experimental observations (figure 3). It should again be noted that the critical values for phase transitions in $PrMn_{2-x}Fe_xGe_2$ may be different from the condition appropriate to pure RMn_2Ge_2 compounds due to electronic effects [6]. Upon further decreasing the temperature to T_C^{Pr}, the Pr moments order and drive the F interplanar coupling of the Mn moments even though the Mn–Mn spacing continues to decrease. The resultant magnetic structure is therefore Fmc for the Mn sublattice with the Pr sublattice showing F order along the c-axis below T_C^{Pr}.

3.1.3. $PrMn_{1.2}Fe_{0.8}Ge_2$. As shown in figure 4, $PrMn_{1.2}Fe_{0.8}Ge_2$ exhibits relatively simple magnetic behaviour compared with $PrMn_{1.6}Fe_{0.4}Ge_2$ and $PrMn_{1.4}Fe_{0.6}Ge_2$ (figures 2 and 3 respectively). The temperature dependences of the magnetization and inverse magnetization are shown in figures 4(a) and (b) respectively, with the magnetization versus field curve at 5 K shown in figure 4(c). On cooling, $PrMn_{1.2}Fe_{0.8}Ge_2$ exhibits a transition from paramagnetism to an intraplanar AF state at $T_N^{intra} \sim 242$ K (this transition is not shown in [7] but is reported in [23]). A subsequent transition to an interlayer AF state occurs at $T_N^{inter} \sim 154$ K as confirmed by our neutron experiments outlined below. The magnetization curve at 5 K displays features characteristic of AF order (figure 4(c)) even though a sudden increase in the magnetization is detected below 20 K (figure 4(a)).

At room temperature, the lattice parameter a (0.4082 nm) of $PrMn_{1.2}Fe_{0.8}Ge_2$ is also larger than the critical value related to condition (i) but the compound is paramagnetic; this indicates that with increasing Fe content the transition from paramagnetism to the AFl state occurs below room temperature. However, with decreasing temperature, $PrMn_{1.2}Fe_{0.8}Ge_2$ transforms

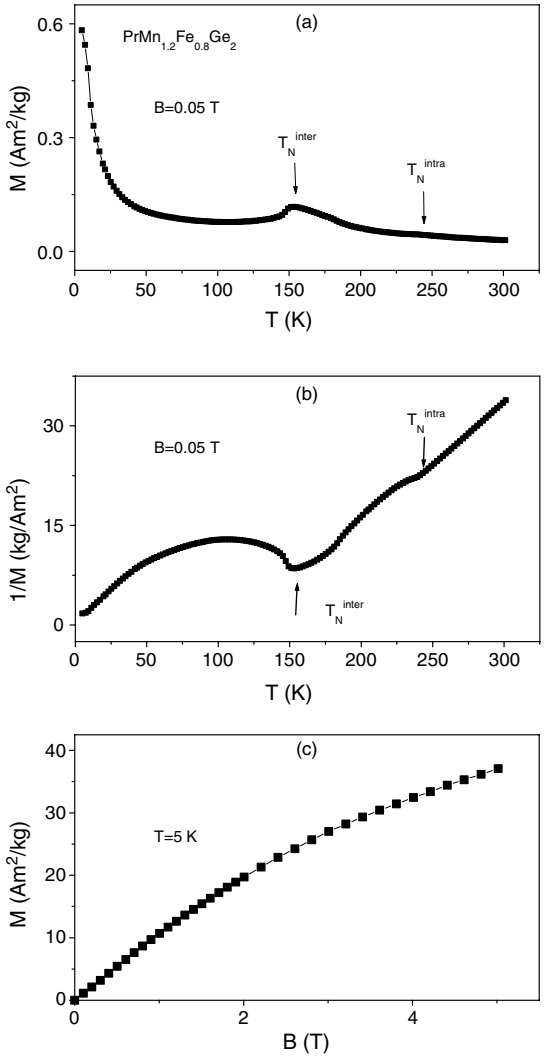

Figure 4. (a) The temperature dependence of magnetization of $PrMn_{1.2}Fe_{0.8}Ge_{2.0}$ (B_{appl} = 0.05 T); (b) the inverse magnetization of $PrMn_{1.2}Fe_{0.8}Ge_{2.0}$ as a function of temperature (B_{appl} = 0.05 T); (c) the magnetization of $PrMn_{1.2}Fe_{0.8}Ge_{2.0}$ as a function of field (B_{appl} = 0–5 T) at 5 K.

directly from the AF*l* state to the AF*mc* state (condition (ii) range) rather than F*mc* even though condition (i) is satisfied in a similar manner to $PrMn_{1.6}Fe_{0.4}Ge_2$ and $PrMn_{1.4}Fe_{0.6}Ge_2$ as mentioned above. This demonstrates that for $PrMn_{1.2}Fe_{0.8}Ge_2$ the electronic effects have changed the critical geometric values associated with the phase transitions as discussed in the introduction.

3.2. Mössbauer studies

Figures 5–7 show the ^{57}Fe Mössbauer spectra of $PrMn_{2-x}Fe_xGe_2$ (x = 0.4, 0.6 and 0.8) at selected temperatures. Full details of the spectral fittings are described below but, in agreement with the magnetic results outlined above, it is evident from the 300 K

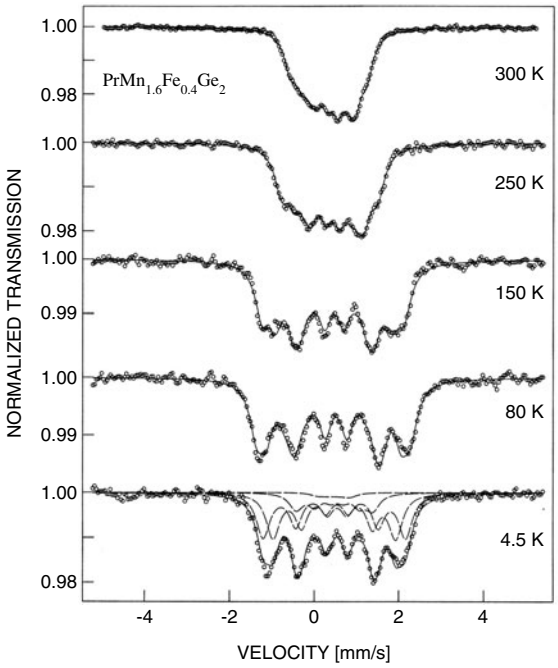

Figure 5. ^{57}Fe Mössbauer spectra of $PrMn_{1.6}Fe_{0.4}Ge_{2.0}$ over the temperature range 4.5–300 K. The fits to the spectra are described in the text.

spectra that $PrMn_{1.2}Fe_{0.8}Ge_2$ is paramagnetic at room temperature while $PrMn_{1.4}Fe_{0.6}Ge_2$ and $PrMn_{1.6}Fe_{0.4}Ge_2$ exhibit magnetic hyperfine splitting; these findings are consistent with our observation of the occurrence of long range AF order in $PrMn_{1.4}Fe_{0.6}Ge_2$ and $PrMn_{1.6}Fe_{0.4}Ge_2$ at room temperature.

Analyses of the Mössbauer spectra of ^{57}Fe doped RT_2X_2 systems have typically been carried out using models based on the random distribution of iron atoms and the possible mutual inter-substitution of the T and X atoms in the $ThCr_2Si_2$-type lattice (e.g. [12, 24, 25]). In the case of the present $PrMn_{2-x}Fe_xGe_2$ samples, the Rietveld refinements to the x-ray diffraction patterns indicate that the ^{57}Fe dopant atoms occupy only the Mn 4d site. Inspection of the magnetically split $PrMn_{2-x}Fe_xGe_2$ spectra in figures 5–7 shows that they cannot be fitted on the basis of a single sextet associated with Fe atoms isolated on the Mn 4d sites; rather, the spectra have been fitted with a model which takes into account the nearest-neighbour (nn) environments. The numbers of nearest-neighbour 2a (R), 4d (T) and 4e (Ge) sites to the 4d sites on which the Fe atoms reside, are four, four and four respectively. Assuming that the Fe atoms occupy the 4d site randomly, the iron atoms would have binomial distributions of nearest-neighbour Mn environments. In the case of $PrMn_{1.6}Fe_{0.4}Ge_2$ for example, a magnetically split spectrum can be represented by four sextets with fractional areas of 0.410, 0.410, 0.154 and 0.027. These sextets represent Fe atoms with zero, one, two and three (or more) nearest-neighbour Fe atoms respectively. The equivalent fractional areas for $PrMn_{1.4}Fe_{0.6}Ge_2$ and $PrMn_{1.2}Fe_{0.8}Ge_2$ are (0.240, 0.412, 0.265, 0.084) and (0.130, 0.346, 0.346, 0.179), respectively.

Figures 5–7 show the fits obtained to the magnetically split $PrMn_{2-x}Fe_xGe_2$ spectra on the basis of this binomial distribution model. Emphasis was placed on fitting the 4.5 K spectrum for each compound, with the final fit parameters then being used as the basis for the initial parameters in analysis of the higher temperature spectra. The fits were obtained with the four

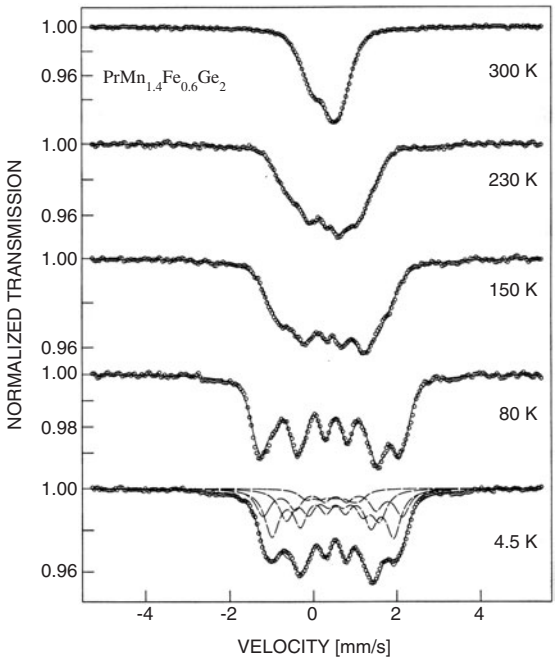

Figure 6. ^{57}Fe Mössbauer spectra of $PrMn_{1.4}Fe_{0.6}Ge_{2.0}$ over the temperature range 4.5–300 K. The fits to the spectra are described in the text.

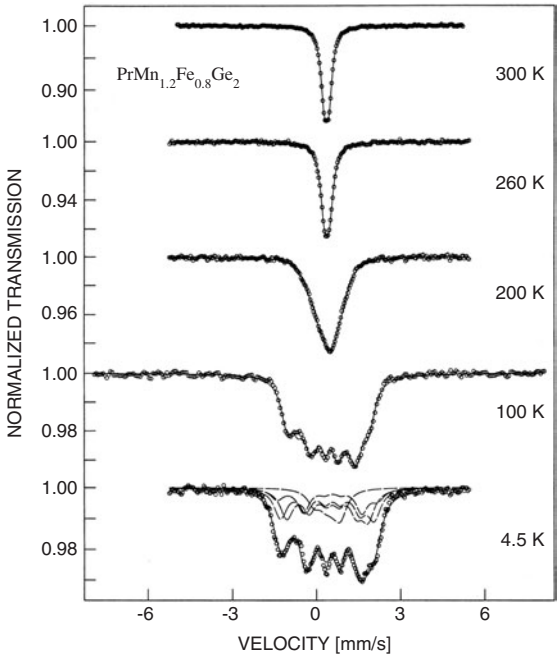

Figure 7. ^{57}Fe Mössbauer spectra of $PrMn_{1.2}Fe_{0.8}Ge_{2.0}$ over the temperature range 4.5–300 K. The fits to the spectra are described in the text.

sub-spectra constrained to the fractional binomial areas as described above and using the same line-width for each sub-spectral component. The magnetic hyperfine field B_{hf} for each sextet component was allowed to vary although, to reduce the number of parameters, and because of the similarity in their values, the isomer shift δ and quadrupole shift ε were varied during the fits but assumed to be the same for each sub-spectral component. Good quality fits were

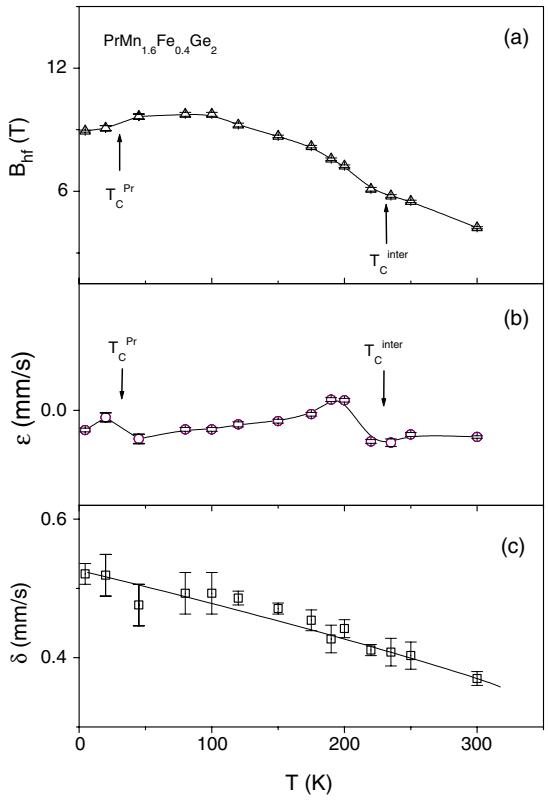

Figure 8. Temperature dependences of the Mössbauer hyperfine parameters of $PrMn_{1.6}Fe_{0.4}Ge_{2.0}$: (a) average magnetic hyperfine field B_{hf}; (b) quadrupole shift ε; (c) isomer shift δ. The arrows show $T_C^{Pr} \sim 30$ K and $T_C \sim 230$ K as discussed in the text.

obtained to the spectra and the nearest-neighbour environment for each sub-spectrum can be assigned by taking into account the influence of the iron atoms on the magnetic hyperfine field and related magnetic moment. As reported elsewhere (e.g. [12, 13]), Fe atoms do not carry a magnetic moment in RFe_2X_2 or in ^{57}Fe doped RT_2X_2 compounds. The present findings are also consistent with the behaviour of Fe as a nonmagnetic probe in $PrMn_{2-x}Fe_xGe_2$. In the case of $PrMn_{1.4}Fe_{0.6}Ge_2$ for example (figure 6), the subspectrum with the largest B_{hf} is attributed to Fe atoms having the largest Mn coordination (i.e. zero Fe nn) and the smallest B_{hf} is attributed to Fe atoms having the largest Fe coordination (three or more nn) in these compounds. Examples of the subspectral components for the three ^{57}Fe doped $PrMn_{2-x}Fe_xGe_2$ compounds are shown in figures 5–7.

3.2.1. $PrMn_{1.6}Fe_{0.4}Ge_2$. Figures 8–10 show the temperature dependence of the Mössbauer hyperfine parameters for $PrMn_{1.6}Fe_{0.4}Ge_2$ and $PrMn_{1.4}Fe_{0.6}Ge_2$ and $PrMn_{1.2}Fe_{0.8}Ge_2$ respectively. As shown by figure 8, the magnetic hyperfine field for $PrMn_{1.6}Fe_{0.4}Ge_2$ exhibits a discontinuity at $T_C \sim 230$ K with a decrease in B_{hf} observed below T_C^{Pr}. As is well known, the observed hyperfine fields result from contributions to the exchange interactions present in the Pr and Mn sublattices and correspondingly reflect the magnetic order in the Pr and Mn sublattices [12, 24, 25]. As discussed above, on decreasing the temperature from room temperature, $PrMn_{1.6}Fe_{0.4}Ge_2$ changes from an antiferromagnetic AF*l* state to a canted ferromagnetic F*mc* state at ∼230 K; it is the additional interlayer ferromagnetic coupling which is responsible for the kink in B_{hf} values around 230 K. The decrease in the B_{hf} values of ^{57}Fe below T_C^{Pr} indicates that the transferred magnetic hyperfine field from the Pr sublattice is

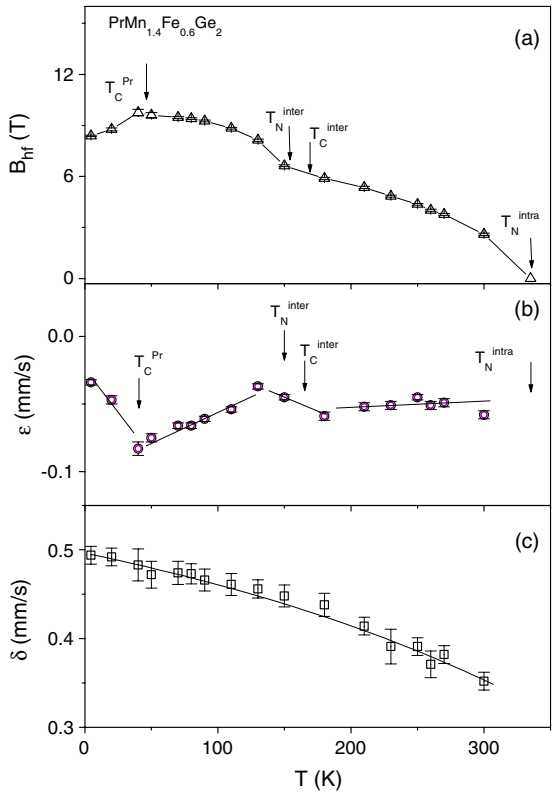

Figure 9. Temperature dependences of the Mössbauer hyperfine parameters of $PrMn_{1.4}Fe_{0.6}Ge_{2.0}$: (a) average hyperfine field B_{hf}; (b) quadrupole shift ε; (c) isomer shift δ. The arrows show $T_C^{Pr} \sim 40$ K, $T_N^{inter} \sim 152$ K and $T_C^{inter} \sim 168$ K as discussed in the text.

opposite to that from the Mn sublattice. This agrees well with the similar behaviour observed in $NdMn_2Ge_2$ and $GdMn_2Ge_2$ [12]. In $GdMn_2Ge_2$ the Gd sublattice orders ferromagnetically at $T_C^{Gd} = 96$ K and forces the Mn to order ferromagnetically and antiparallel to the Gd magnetization, thus resulting in net ferrimagnetic-like behaviour [12]. The decrease in the B_{hf} of ^{57}Fe in $GdMn_2Ge_2$ below the ordering of the Gd sublattice indicates that the transferred magnetic hyperfine field from the Gd sublattice is opposite to that contributed from the Mn sublattice. In the case of $PrMn_{1.6}Fe_{0.4}Ge_2$ however, it was suggested from magnetization measurements that the Pr sublattice aligns ferromagnetically with the Mn magnetization [7]. Given such a ferromagnetic interaction, the decrease in the B_{hf} values below T_C^{Pr} (figure 8(a)) is surprising and needs clarification. On the other hand a discontinuity in the quadrupole shift ε at the magnetic phase transition temperatures has been observed, which may be due to a possible distortion of the unit cell and/or the variation in the magnetic ordering of the Mn moment. These points will be clarified in our continuing neutron diffraction investigation.

3.2.2. $PrMn_{1.4}Fe_{0.6}Ge_2$. In the case of $PrMn_{1.4}Fe_{0.6}Ge_2$, the average hyperfine field (figure 9(a)) behaves generally in a similar manner to the magnetization curves of figure 3(a). The temperatures at which pronounced changes in the magnetic hyperfine fields are observed agree well with the magnetic transition temperatures $T_C^{Pr} \sim 40$ K, $T_N^{inter} \sim 152$ K and $T_C^{inter} \sim 168$ K as derived from the magnetization measurements. The decrease in B_{hf} at $\sim$150 K coincides well with the transition from the low temperature antiferromagnetic state to the ferromagnetic state at $T_N^{inter} \sim 152$ K and, as in the case of $PrMn_{1.6}Fe_{0.4}Ge_2$, a sudden decrease in B_{hf} below T_C^{Pr} has again been observed. Changes in the trends of the ε as derived

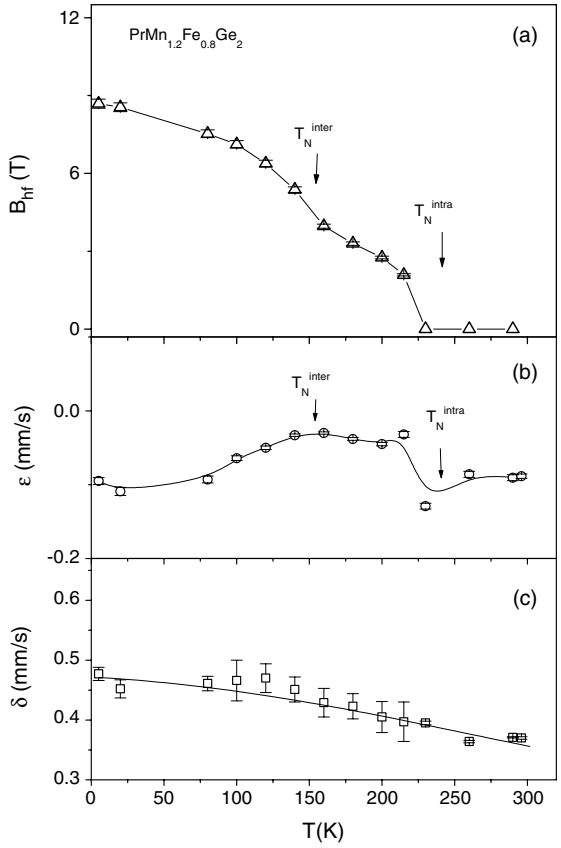

Figure 10. Temperature dependences of the Mössbauer hyperfine parameters of $PrMn_{1.2}Fe_{0.8}Ge_{2.0}$: (a) average hyperfine field B_{hf}; (b) quadrupole shift ε; (c) isomer shift δ. The arrows show $T_N^{inter} \sim 154$ K and $T_N^{intra} \sim 242$ K as discussed in the text. For $T > T_N^{intra}$, the quadrupole shift ε is obtained from the quadrupole splitting Δ ($\varepsilon = \Delta/2$ here).

from the spectral fits (figure 9(b)) correlate well with the magnetic transition temperatures derived earlier (figure 3(a)). As discussed elsewhere [5, 25], this behaviour may be related to the relative orientation (angle θ) of V_{zz}, the principal component of the electric field gradient (EFG) tensor and the Mn magnetic moment (and hence the magnetic hyperfine field experienced by the ^{57}Fe nuclei) due to the variation of Mn magnetic structure and/or the anisotropic change of the lattice parameters at the transition temperatures. Such anisotropic behaviour of the lattice parameters was detected in $SmMn_2Ge_2$ through the magnetic transitions, with a larger change in the a lattice parameter being observed, compared with the c lattice parameter [21, 22].

3.2.3. $PrMn_{1.2}Fe_{0.8}Ge_2$. Figure 10 shows the temperature dependence of the hyperfine parameters for $PrMn_{1.2}Fe_{0.8}Ge_2$. The absence of a magnetic hyperfine splitting above $T_N^{intra} \sim 242$ K (see also figure 7) confirms that this temperature corresponds to a transition from antiferromagnetism to paramagnetism while persistence of the magnetic hyperfine splitting below $T_N^{inter} \sim 154$ K corresponds to the transition from intra-AF to inter-AF at lower temperatures. Again, the variation of the ε values correlate with the transition temperatures determined from the magnetic measurements of figure 4. For $T > T_N^{intra}$, the quadrupole shift ε is derived from the quadrupole splitting Δ ($\varepsilon = \Delta/2$ here).

3.3. Neutron studies

An initial set of neutron powder diffraction patterns has been obtained for $PrMn_{1.2}Fe_{0.8}Ge_2$ and Rietveld refinements carried out using the FULLPROF program package [16] which

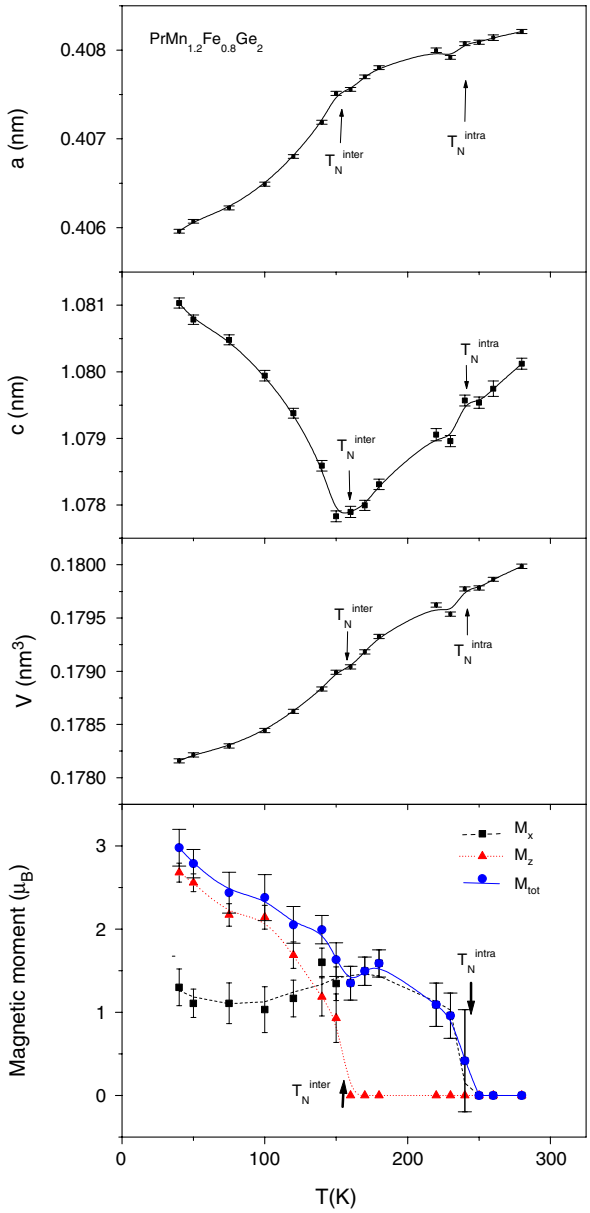

Figure 11. The variation of the a and c lattice parameters, the unit cell volume V and the magnetic moments for $PrMn_{1.2}Fe_{0.8}Ge_{2.0}$ as determined by neutron diffraction measurements over the temperature range ∼20–300 K. The M_x and M_z components of the total magnetic moment are shown for the AFmc magnetic structure below $T_N^{inter} \sim 154$ K. The arrows show $T_N^{inter} \sim 154$ K and $T_N^{intra} \sim 242$ K as discussed in the text.

allows simultaneous refinement of the structural and magnetic parameters. Figure 11 shows the variation of the unit cell parameters and magnetic moments of $PrMn_{1.2}Fe_{0.8}Ge_2$ with temperature over the range 20–300 K. No coherent magnetic scattering was observed in $PrMn_{1.2}Fe_{0.8}Ge_2$ at room temperature as expected on the basis of the magnetization (figure 4) and ^{57}Fe Mössbauer results (figure 7). Below $T_N^{intra} \sim 242$ K and in good agreement with the recent findings of Dincer *et al* [23], $PrMn_{1.2}Fe_{0.8}Ge_2$ exhibits AF ordering within (001) Mn layers and the AFl structure as depicted in figure 1. With further decreases in temperature the AF mixed commensurate magnetic structure AFmc is formed below $T_N^{inter} \sim 154$ K, leading to the M_x and M_z components of the total magnetic moment as shown in figure 11. It is also

evident from figure 11 that in the interplanar AF region below T_N^{inter}, the a lattice parameter is reduced significantly while the c lattice parameter is increased, whereas the onset of intraplanar AF coupling at $T_N^{intra} \sim 242$ K is characterized by slight decreases in both the a and c lattice parameters.

4. Conclusions

Substitution of Fe for Mn leads to a distinct decrease in the lattice constants and unit cell volume. The $PrMn_{1.6}Fe_{0.4}Ge_2$ and $PrMn_{1.4}Fe_{0.6}Ge_2$ samples are antiferromagnetic at room temperature whereas $PrMn_{1.2}Fe_{0.8}Ge_2$ is paramagnetic. $PrMn_{1.4}Fe_{0.6}Ge_2$ exhibits re-entrant ferromagnetism below $T_C^{Pr} \sim 40$ K. The temperature dependences of the hyperfine parameters for $PrMn_{1.4}Fe_{0.6}Ge_2$ and $PrMn_{1.2}Fe_{0.8}Ge_2$ exhibit changes at the phase transition temperatures determined from the magnetic measurements (figures 7 and 8). The transferred hyperfine field at the ^{57}Fe nucleus in $PrMn_{1.4}Fe_{0.6}Ge_2$ is smaller at 4.5 K (below the ordering temperature of Pr) than at 50 K (above T_C^{Pr}), thus establishing that the transferred hyperfine field from Pr is opposite to that produced by Mn. An anisotropic thermal expansion occurs with interplanar antiferromagnetic coupling range for $PrMn_{1.2}Fe_{0.8}Ge_2$.

Acknowledgments

This work is supported by a Discovery Grant from the Australian Research Council leading to the award of a Research Associateship to JLW. The work is also supported in part by a grant from the Australian Institute of Nuclear Science and Engineering.

References

[1] Szytula A and Leciejewicz J 1988 *Handbook on the Physics and Chemistry of Rare Earths* vol 12, ed K A Gschneidner Jr and L Eyring (Amsterdam: Elsevier) p 133
[2] Szytula A and Leciejewicz J 1994 *Handbook on Crystal Structures and Magnetic Properties of Rare Earth Intermetallics* (Boca Raton, FL: CRC Press)
[3] Welter R and Malaman B 2003 *J. Alloys Compounds* **354** 35
[4] Dincer I, Elerman Y, Elmali A, Ehrenberg H, Fuess H, Duman E and Acet M 2002 *J. Magn. Magn. Mater.* **248** 268
[5] Venturini G, Welter R, Ressouche E and Malaman B 1995 *J. Magn. Magn. Mater.* **150** 197
[6] Venturini G, Malaman B and Ressouche E 1996 *J. Alloys Compounds* **237** 61
[7] Kervan S, Elerman Y, Elmali A and Theissmann R 2001 *J. Alloys Compounds* **327** 27
[8] Dincer I, Elerman Y, Elmali A, Ehrenberg H and Fuess H 2002 *J. Alloys Compounds* **334** 72
[9] Wang Y G, Yang F M, Chen C P, Tang N and Wang Q D 1997 *Phys. Status Solidi* a **162** 723
[10] Dirkmaat A J, Endstra T, Knetsch E A, Menovsky A A, Nieuwenhuys G J and Mydosh J A 1990 *J. Magn. Magn. Mater.* **84** 143
[11] Venturini G, Welter R, Ressouche E and Malaman B 1994 *J. Alloys Compounds* **210** 209
[12] Nowik I, Levi Y, Felner I and Bauminger E R 1995 *J. Magn. Magn. Mater.* **147** 373
[13] Malaman B, Venturini G, Blaise A, Sanchez J P and Amoretti G 1993 *Phys. Rev.* B **47** 8681
[14] Welter R, Venturini G, Ressouche E and Malaman B 1995 *J. Alloys Compounds* **218** 204
[15] Venturini G, Welter R, Ressouche E and Malaman B 1994 *J. Alloys Compounds* **210** 213
[16] Rodriguez-Carvajal J 1990 *The XV-th Congr. Int. Union of Crystallography, Proc. Satellite Mg On Powder Diffraction (Toulouse, France)* p 127 http://www-llb.cea.fr/fullweb/
[17] Gelato L 1981 *J. Appl. Crystallogr.* **14** 151
[18] Jacobs J T H, Buschow K H J, Verhoef R and de Boer F R 1990 *J. Less-Common Met.* **157** L11
[19] Fujii H, Okamoto T, Shigeoka T and Iwata N 1985 *Solid State Commun.* **53** 715
[20] Duraj M, Duraj R and Szytula A 1989 *J. Magn. Magn. Mater.* **82** 319
[21] Tomka G J, Kapusta Cz, Ritter C, Riedi P C, Cywinski R and Buschow K H J 1997 *Physica* B **230** 727
[22] Tomka G J, Ritter C, Riedi P C, Kapusta Cz and Kocemba W 1998 *Phys. Rev.* B **58** 6330
[23] Dincer I, Elerman Y, Elmali A, Ehrenberg H, Fuess H and Andre G 2004 Poster presentation, unpublished results
[24] Nowik I, Felner I and Bauminger E R 1997 *Phys. Rev.* B **55** 3033
[25] Campbell S J, Cadogan J M, Zhao X L, Hofmann M and Li H S 1999 *J. Phys.: Condens. Matter* **11** 7835